The effects of aging on male mouse pancreatic β-cell function involve multiple events in the regulation of secretion: influence of insulin sensitivity.

Eva Tudurí[1,2,*], PhD, Sergi Soriano[2,3], PhD, Lucía Almagro[2], MS, Anabel García-Heredia[2], PhD, Alex Rafacho[4], PhD, Paloma Alonso-Magdalena[1,2], PhD, Ángel Nadal[1,2], PhD, Ivan Quesada[1,2,*], PhD.

[1]Spanish Biomedical Research Centre in Diabetes and Associated Metabolic Disorders (CIBERDEM), Madrid, Spain.

[2]Instituto de Investigación, Desarrollo e Innovación en Biotecnología Sanitaria de Elche (IDiBE), Universidad Miguel Hernández de Elche, Elche, Spain.

[3]Departamento de Fisiología, Genética y Microbiología, Universidad de Alicante, Alicante, Spain.

[4]Department of Physiological Sciences, Center of Biological Sciences, Federal University of Santa Catarina, Florianopolis, Brazil.

*Corresponding etuduri@umh.es; ivanq@umh.es

Abstract

Aging is associated with a decline in peripheral insulin sensitivity and an increased risk of impaired glucose tolerance and type 2 diabetes. During conditions of reduced insulin sensitivity, pancreatic β-cells undergo adaptive responses to increase insulin secretion and maintain euglycemia. However, the existence and nature of β-cell adaptations and/or alterations during aging are still a matter of debate. In this study, we investigated the effects of aging on β-cell function from control (3-month-old) and aged (20-month-old) mice. Aged animals were further categorized in two groups: high insulin sensitive (aged-HIS) and low insulin sensitive (aged-LIS). Aged-LIS mice were hyperinsulinemic, glucose intolerant and displayed impaired glucose-stimulated insulin and C-peptide secretion, whereas aged-HIS animals showed characteristics in glucose homeostasis similar to controls. In isolated β-cells, we observed that glucose-induced inhibition of K_{ATP} channel activity was reduced with aging, particularly in the aged-LIS group. Glucose-induced islet NAD(P)H production was decreased in aged mice, suggesting impaired mitochondrial function. In contrast, voltage-gated Ca^{2+} currents were higher in aged-LIS β-cells, and pancreatic islets of both aged groups displayed increased glucose-induced Ca^{2+} signaling and augmented insulin secretion compared with controls. Morphological analysis of pancreas sections also revealed augmented β-cell mass with aging, especially in the aged-LIS group, as well as ultrastructural β-cell changes. Altogether, these findings indicate that aged mouse β-cells compensate for the aging-induced alterations in the stimulus-secretion coupling, particularly by adjusting their Ca^{2+} influx to ensure insulin secretion. These results also suggest that decreased peripheral insulin sensitivity exacerbates the effects of aging on β-cells.

Keywords: pancreatic β-cell, aging, insulin secretion, K_{ATP} channels, Ca^{2+} signalling

INTRODUCTION

Due to the global rise in life expectancy, in recent years there has been a notable increase in diseases related to aging . At the metabolic level, aging is associated with a decline in the accurate management of glucose homeostasis, which may result in impaired glucose tolerance (IGT) and/or type 2 diabetes (T2D) . Indeed, according to the International Diabetes Federation, the highest prevalence of diabetes is observed in the older adults . Although the exact contribution of aging *per se* to impaired glucose homeostasis in older subjects is not yet fully elucidated, it probably involves both senescence-derived effects and age-related factors such as changes in body composition, physical activity and dietary habits, among others . In physiological and pathological conditions of decreased peripheral insulin sensitivity, the endocrine pancreas undergoes several morphofunctional adaptations to adjust plasma insulin levels to the requirements imposed by insulin resistance (IR) . The progression from normal glucose tolerance to T2D has been traditionally viewed as a failure of pancreatic β-cells to fully compensate for IR . An age-associated decrease in peripheral insulin sensitivity along with altered glucose homeostasis has been documented in both humans and mice . Impaired insulin signaling with aging has been also reported in several human and rodent tissues involved in glucose metabolism such as the skeletal muscle, the liver, the adipose tissue, and the nervous system .

Since the progression towards IGT and T2D in a context of IR conditions requires β-cell dysfunction and insufficient compensatory adaptation, several studies have aimed to investigate β-cell responses during aging. Different reports performed in rodent models have shown increased β-cell mass at advanced ages , which has been inferred as an adaptive response to IR. However, the findings related to β-cell function in aged animals present a

high degree of heterogeneity. In mice, while some studies reported an age-dependent decline in glucose-stimulated insulin secretion (GSIS) , other articles described no changes or even improved β-cell responses . In addition to differences in the experimental procedures or the animal strains, these heterogeneous results might be due to other different factors. A limitation in most studies is that aged mice have been analyzed without considering the potential effect of age-associated changes in peripheral insulin sensitivity on islet function, which should affect glucose homeostasis and β-cell secretion. Furthermore, in the current literature there are significant variations in the ages studied from juvenile to middle and advanced ages, which may lead to confounding conclusions . To consider these aspects, in the present study we have analyzed the *in vivo* and *ex vivo* function of pancreatic β-cells in control (3-month-old) and aged (20-month-old) mice, being the latter categorized into two groups according to their degree of insulin sensitivity. Our results indicate that, although aged mouse β-cells present several alterations in the stimulus-secretion coupling, they are able to compensate for these changes, adjusting Ca^{2+} signaling and insulin secretion. These adaptations, however, are not sufficient to avoid IGT in the aged animals with lower degree of peripheral insulin sensitivity.

MATERIAL AND METHODS

Animals: Young adult (3-month-old ± 2 weeks, controls) and aged (20-month-old ± 2 weeks) C57BL/6 male mice were kept under controlled and standardized conditions with a light/dark cycle of 12 h, 22 °C and *ad libitum* access to food and water. All the procedures were evaluated and approved by the Animal Ethics Committee of our institution in accordance with current national and European legislation. Animals were supplied by the institution's animal experimentation service generally in batches of 5-6 mice from both ages at a time. C57BL/6 mice were obtained from Envigo (C57BL/6JOlaHsd; Barcelona, Spain) for breeding protocols. Then, the animals were maintained in the animal experimentation service of our institution.

HOMA-IR and QUICKI: HOMA-IR and QUICKI were calculated as previously described . Briefly, HOMA-IR was calculated as (G_0 x I_0)/adjusted mouse factor. The adjusted mouse factor was calculated for each batch of mice as averaged G_0 x I_0 of the control group to substitute the normalizing human factor of the original HOMA-IR equation. QUICKI was calculated as 1/[log (G_0) + log (I_0)], where G_0 (mg/dL) and I_0 (µU/mL) represent 6 h fasting blood glucose and plasma insulin, respectively. Aged mice were categorized into high insulin sensitive (HIS) or low insulin sensitive (LIS) based on whether their individual QUICKI index fell over (LIS) or below (HIS) the 25th percentile of the corresponding averaged QUICKI value of the control group, respectively .

Intraperitoneal glucose and insulin tolerance tests, and *in vivo* glucose-stimulated insulin secretion (GSIS): Mice were fasted for 6 h (9:00 to 15:00) and then intraperitoneally injected with either glucose (2 g/kg body weight (b.w.) for glucose tolerance test (GTT) and GSIS) or insulin (0.7 UI/kg b.w. for the insulin tolerance test (ITT)). Blood was sampled from the tail vein for glucose measurements during GTT and ITT, and from the saphenous vein for glucose, insulin and C-peptide during GSIS. Glycaemia was monitored using an automatic glucometer (Accu-Chek Compact plus, Roche, Madrid, Spain). Plasma insulin and C-peptide levels were determined by ELISA (Crystal Chem, Downers Grove, IL).

Islet isolation and cell culture: Mice were euthanized by cervical dislocation, and islets were isolated by collagenase digestion . In some assays, isolated islets were dispersed into single cells by trypsin enzymatic digestion and then cultured overnight at 37°C in RPMI 1640 (Gibco, Thermo Fisher Scientific Inc., Carlsbad, CA) supplemented with 10% fetal calf serum, 100 IU/mL penicillin, 0.1 mg/mL streptomycin and 11 mM D-glucose . Islets and/or pancreatic beta-cells were individually examined in the experiments of electrical activity, NAD(P)H measurements, Ca^{2+} signaling and transmission electronic microscopy (TEM). Groups of islets from the same animal were employed for *ex vivo* insulin secretion, mRNA extraction, and TEM sample preparation. Islets from different mice were not pooled.

***Ex vivo* GSIS and insulin content measurements:** Freshly isolated islets were left to recover at 37ºC for 2 h. Afterwards, batches of 15 size-matched islets were transferred to a 24-well plate with Millicell® Cell Culture Inserts (Merk, Darmstadt, Germany) immersed in 500 µL of a solution containing (in mM): 140 NaCl, 4.5 KCl, 2.5 $CaCl_2$, 1 $MgCl_2$, 20 HEPES, and D-glucose (0.5 or 11 mM), pH=7.35, and left at 37 ºC and 5% CO_2 to secrete for 1 h. Afterwards, the medium was collected and frozen for subsequent insulin measurements using ELISA (Mercodia, Uppsala, Sweden). Then, islets were handpicked and transferred to

20 µL of ethanol/HCl buffer and incubated overnight at 4ºC for further quantification of insulin content. Protein concentration was measured by the Bradford dye method .

Ca^{2+} and NAD(P)H imaging: Isolated islets were allowed to recover for 2 h at 37 ºC, incubated for 1 h at room temperature (RT) with 5 µM Fura 2-AM (Invitrogen, Thermo Fisher Scientific Inc., Carlsbad, CA), and then transferred to an imaging chamber mounted on a Zeiss Axiovert 200 inverted microscope (Zeiss, Jana, Germany) equipped with a 40X objective. During the experiments, islets were continuously perifused with a solution containing (in mM): 120 NaCl, 5 KCl, 2.5 $CaCl_2$, 1.1 $MgCl_2$, 25 $NaHCO_3$ (pH=7.35). Images were acquired every 2.5 s using a Hamamatsu C9100 digital camera and the Aquacosmos 2.6 software (Hamamatsu Photonics, Hamamatsu, Japan). Fluorescence measurements were obtained at excitation wavelengths of 340 and 380 nm. Cytosolic Ca^{2+} changes were expressed as the ratio of the fluorescence at 340 and 380 nm . The increase in fluorescence ($\Delta F_{340/380}$) was obtained by subtracting the basal fluorescence from the fluorescence value recorded during the peak signal induced by the stimuli. The area under the curve (AUC) was calculated during the last 5 min of high glucose application . NAD(P)H levels were monitored as changes in autofluorescence using a 365 nm band-pass excitation filter and a 445 ± 50 nm emission filter. Fluorescence changes were analyzed as previously reported .

Electrophysiological recordings: K_{ATP} channel activity was recorded using standard patch-clamp recording procedures from isolated β-cells in cell-attached configuration, as previously described . Around 80-90% of the single cells were identified as β-cells by their electrical response to glucose. For the patch-clamp recordings of voltage-gated K^+ and Ca^{2+} currents, the standard whole-cell patch-clamp configuration was used, as previously described . Pancreatic β-cells were identified by size (>5 pF) and the corresponding steady-state inactivation properties of the tetrodotoxin (TTX)-sensitive Na^+ current (29). Data were

obtained using an Axopatch 200B patch-clamp amplifier (Axon Instruments Co. CA, USA). Patch pipettes were pulled from borosilicate capillaries (Sutter Instruments Co. CA, USA) using a flaming/brown micropipette puller P-97 (Sutter Instruments Co. CA, USA) and heat polished at the tip using a MF-830 microforge (Narishige, Japan). The bath solution contained (in mM): 135 NaCl, 5 KCl, 2.5 $CaCl_2$, 1.1 $MgCl_2$, 10 HEPES and 10 glucose (pH 7.4 with NaOH). The pipette solution contained (in mM): 140 KCl, 2.7 $CaCl_2$, 0.6 $MgCl_2$, 10 EGTA, 5 MgATP and 10 HEPES (pH 7.2 with KOH). After filling the pipette with the pipette solution, the pipette resistance was 3–5 MΩ. A tight seal (>1 GΩ) was established between the β-cell membrane and the tip of the pipette by gentle suction. The series resistance of the pipette usually increased to 6–15 MΩ after moving to whole-cell. Series resistance compensation was used (up to 70%) for keeping the voltage error below 5 mV during current flow. Data were filtered (2 kHz) and digitized (10 kHz) using a Digidata 1322 A (Axon Instruments Co. CA, USA) and stored in a computer for subsequent analysis using commercial software (pClamp9, Axon Instruments Co. CA, USA). All experiments were carried out at 32–34 °C.

Immunohistochemistry: Once removed, pancreata were weighted and fixed with ice-cold 4% paraformaldehyde for 20 h at 4 ºC. Afterwards, pancreata were embedded in paraffin, and sections (5 µm) were cut 200 µm apart. To study β-cell mass, antigen retrieval was performed by heating the samples for 20 min in citrate buffer (10 mM, pH 6.0), and the blockade was done by incubation for 2 h in 3% BSA in PBS at RT. Samples were incubated overnight at 4ºC with a rabbit anti-insulin antibody (1:200, C27C9, Cell Signalling, USA) and, then, with biotinylated goat anti-rabbit IgG (H+L) (Zymed, BA 9200, Vector laboratories, Burlingame, CA, USA). Samples were mounted with Vitro-Clud Mounting Medium (Deltalab, Barcelona, Spain), and were imaged at 4x and at 20x for quantification of the total pancreatic area and insulin immunostained area, respectively. β-cell area was calculated by measuring the total

insulin-stained area normalized by the total pancreatic area using the Metamorph Software (Molecular Devices, San Jose, CA, USA). β-cell mass was calculated by multiplying the β-cell area (%) by the pancreas weight (30).

Apoptosis and β-cell proliferation analysis by immunofluorescence: Apoptotic β-cells were analyzed by the TUNEL technique (In Situ Cell Death Detection Kit, Roche, Switzerland) as previously described following manufacturer's instructions for difficult tissue. Samples were blocked for 2 h before incubation with the primary antibody rabbit anti-insulin antibody (1:200, C27C9, Cell Signalling, USA) at 4°C overnight, and with Alexa Fluor 546 (1:500, Life technologies, Carlsbad, CA, USA) for 2 h at RT. For the analysis of proliferation, a mouse anti-insulin antibody (1:200, Cat. I2018, Sigma, USA) and a rabbit anti-Ki67 antibody (1:400, Cat. 9129, Cell Signalling Technology, Danvers, MS, USA) were used. Pancreas sections were incubated overnight at 4ºC in the presence of both primary antibodies, and then with Alexa Fluor 546 and 488 (1:500, Life technologies, USA) for 2 h at RT. Nuclei were stained with Hoechst 33342 (1:1000; Invitrogen, Barcelona, Spain). Images were acquired with an IN Cell Analyzer 6000 system (GE Healthcare, Little Chalfont, UK), and analysis was performed with ImageJ software (National Institutes of Health, Bethesda, MD, USA).

Transmission electronic microscopy (TEM): Freshly isolated pancreatic islets were processed using a standard Spurr protocol as previously described . Thin sections were cut in an ultramicrotome (Leica UC7; Leica Microsystems, Germany). TEM images were taken with an EMCCD camera (TRS 2k x 2k) in a Zeiss Libra 120 transmission electron microscope operating at 80 kV. A minimum of 10 TEM images obtained from control and aged islets (n=3 mice/group) were analyzed using ImageJ software (National Institutes of Health, Bethesda, MD, USA).

RNA isolation and gene expression analysis by RT-qPCR: Total RNA was extracted with RNeasy Micro Kit (Qiagen, Madrid, Spain) according to the manufacturer's instructions and quantified with a Nanodrop 2000 (Thermo Fisher Scientific, Waltham, MA, USA), followed by cDNA synthesis with High capacity cDNA reverse transcription kit (Applied Biosystems, Foster City, CA, USA). Quantitative RT-PCR (qRT-PCR) assays were performed in a final volume of 10 µL, with 1 µL of cDNA, 200 nM of each primer and 1 x IQ™ SYBR® Green Supermix (Bio-Rad, Hercules, CA, USA), in a CFX96 Real Time System (Bio-Rad, Hercules, CA, USA). Relative values were calculated by the Pfaffl method . Primer sequences are described in Supplementary Table 1.

Statistical analysis: After testing for normality, we performed one-way ANOVA, or two-way ANOVA when required, followed by post hoc Tukey test when variables were normally distributed, and Kruskal–Wallis test, followed by Dunn's multiple comparisons test, when variables were not normally distributed. Tests were performed with Prism (GraphPad Software v7). Data are presented as mean ± SEM, and statistical significance was set at $p<0.05$ for all analyses.

RESULTS

Aged-LIS mice display hyperinsulinemia, glucose intolerance and impaired *in vivo* glucose-stimulated insulin secretion (GSIS).

Since aging has been associated with changes in peripheral insulin sensitivity and glucose tolerance , we aimed to firstly categorize aged animals according to their degree of insulin sensitivity using the QUICKI index. As shown in Figure 1A, while aged-LIS animals presented lower QUICKI values, this surrogate measure of insulin sensitivity was similar between aged-HIS mice and young controls. The HOMA-IR index also led to similar conclusions (Fig. 1B). In agreement with both indexes, lower insulin sensitivity was also

observed in aged-LIS animals during an insulin tolerance test (Fig. 1C). Both groups of aged mice showed increased body weight compared to the control group (Supplementary Fig. 1).

Blood glucose levels in all groups were within a physiological range after 6 h fasting , despite a modest but lower glycemic value registered in aged-HIS mice (Fig. 1D). Fasting insulinemia, however, was remarkably higher in the aged-LIS group compared to both control and aged-HIS animals (Fig. 1E). In response to an intraperitoneal glucose load, only aged-LIS mice displayed impaired glucose tolerance (Fig. 1F). This was probably associated with altered insulin release in this group: while control and aged HIS-mice displayed augmented plasma insulin levels within 10 minutes following an intraperitoneal glucose load (Fig. 1G), aged LIS-mice were not able to increase insulin levels during this period. Because plasma insulin does not only depend on insulin secretion but also on insulin clearance, we also quantified plasma C-peptide levels to better characterize *in vivo* β-cell function. In addition to higher basal insulinemia (Fig. 1G), aged-LIS mice presented higher basal C-peptide values (Fig. 1H). Moreover, whereas control and aged-HIS mice augmented C-peptide levels immediately following the glucose load (Fig. 1H), this effect was delayed in aged-LIS animals, confirming the impaired insulin secretion in this latter group. All these findings indicate that aged-HIS mice presented a phenotype similar to controls in terms of glucose homeostasis, while aged-LIS animals exhibited glucose intolerance, basal hyperinsulinemia, lower insulin sensitivity and impaired *in vivo* insulin release.

Aged-LIS β-cells display reduced glucose-induced inhibition of K_{ATP} channel activity.

After the metabolic characterization of the three experimental groups, we aimed to analyze β-cell function, examining the different signaling events involved in GSIS. Increased cytosolic ATP levels derived from glucose metabolism close K_{ATP} channels, which control the resting membrane potential, producing β-cell membrane depolarization. This

depolarization triggers action potentials by opening of voltage-gated Ca^{2+} channels, increasing intracellular Ca^{2+} levels, which induce the exocytosis of insulin granules .

Using the patch-clamp technique, we studied K_{ATP} channel activity in isolated β-cells. Figure 2A shows basal K_{ATP} channel activity at low glucose concentration (0.5 mM) in control, aged-HIS and aged-LIS β-cells. Increasing glucose concentration from 0.5 to 11 mM reduced K_{ATP} channel activity, while application of diazoxide reactivated K_{ATP} channels in the three groups (Fig. 2A-B and Supplementary Fig. 2A). Remarkably, while 11 mM glucose decreased K_{ATP} channel activity by ~94% relative to 0.5 mM glucose in controls, it was only reduced by ~80% and ~43% in aged-HIS and aged-LIS β-cells, respectively (Fig. 2B). Despite this lower inhibitory effect in the aged groups, the application of 11 mM glucose was sufficient to depolarize the plasma membrane and trigger action potentials in both aged β-cells and controls, as manifested by the generation of action currents (Fig. 2A, inset: 6 min after application of 11 mM glucose). Basal K_{ATP} channel open probability (0.5 mM glucose) tended to be higher in aged groups compared to controls (Supplementary Fig. 2A). Gene expression analysis of the two subunits that form the K_{ATP} channel, Sur1 (*Abcc8*) and Kir6.2 (*Kcnj11*), revealed no differences among groups (Supplementary Fig. 2B), indicating that altered K_{ATP} channel function in aged β-cells might be independent of transcriptional regulation.

Glucose-induced K_{ATP} channel blockade depends on increasing cytosolic ATP concentrations. Glucose metabolism increases NAD(P)H levels, which are required for mitochondrial ATP synthesis. In this regard, the reduced effect of glucose on K_{ATP} channel closure in aged β-cells could be associated with alterations in glucose metabolism. To analyze β-cell glucose metabolism, NAD(P)H-derived fluorescence responses were measured in isolated islets exposed to low (0.5 mM) and high (11 mM) glucose, as well as sodium azide (NaN_3) to induce a maximal $NAD(P)^+$ reduction (Fig. 2C). These experiments showed that

the glucose-induced increase in islet NAD(P)H levels was similarly impaired in both aged groups (Fig. 2D), indicating that aging *per se* affects β-cell glucose metabolism. Altogether, these results suggest that the alterations observed in K_{ATP} channel activity from aged β-cells could be derived from impaired glucose metabolism.

Aged-LIS β-cells exhibit enhanced voltage-gated Ca^{2+} currents.

Given the voltage-dependence of the pancreatic β-cell electrical activity, we analyzed voltage-gated K^+ and Ca^{2+} currents in isolated β-cells to seek for potential alterations during aging. Using the patch-clamp technique, currents were elicited by pulses ranging from -60 to +80 mV from a holding potential of -70 mV (Fig. 3A). As shown in Figure 3B, voltage-gated K^+ currents were similar in the three groups. In line with this, no significant differences were observed in the gene expression levels of the voltage-gated delayed-rectifier $K_V2.1$ channel (*Kcnb1*) (Supplementary Fig. 2B). This channel accounts for most of the delayed outward current in mouse β-cells and plays a key role in action potential repolarization . In the case of voltage-gated Ca^{2+} currents, these were slightly augmented in aged-HIS β-cells and significantly larger in aged-LIS β-cells compared with controls (Fig. 3C). Similar mRNA levels were found in the three groups for the voltage-gated L-type Ca^{2+} channel (*Cacna1c*; Cav1.2 alpha 1C subunit), which is a major conduit for extracellular Ca^{2+} entry and plays a major role in both action potential generation and GSIS (Supplementary Fig. 2B). Likewise, no differences were detected in the expression of the voltage-gated N-type Ca^{2+} channel (*Cacna1b*; Cav2.2 alpha 1B subunit). These findings suggest that increased voltage-gated Ca^{2+} currents during aging are probably regulated by mechanisms other than gene transcription.

Glucose-induced intracellular Ca^{2+} signaling is enhanced in aged β-cells.

To further explore the key events in the β-cell stimulus-secretion coupling during aging, we next analyzed intracellular Ca^{2+} signals in isolated pancreatic islets. Islets were exposed to low (0.5 mM) and high (11 mM) extracellular glucose concentrations, as well as depolarizing conditions (30 mM KCl) (Fig. 3D). As shown in Figure 3E, basal fluorescence was similar in the three groups. Both the amplitude and the AUC of the glucose-induced Ca^{2+} signals were increased in both groups of aged islets compared to controls (Fig. 3F,G). Furthermore, both aged groups displayed higher Ca^{2+} responses than controls when stimulated with KCl, although only aged-HIS islets showed statistical significance (Fig. 3H). The analysis of different regions within each individual islet showed the characteristic β-cell Ca^{2+} synchrony in the three groups (Supplementary Fig. 3), indicating that cell-to-cell communication was not compromised during aging. Overall, these findings are in line with those of the voltage-gated Ca^{2+} currents and indicate that Ca^{2+} signaling improved in aged β-cells.

GSIS is enhanced in aged β-cells.

GSIS from β-cells is a Ca^{2+}-dependent process . *Ex vivo* analysis of GSIS showed that isolated islets exposed to stimulatory (11 mM) glucose concentrations presented enhanced insulin secretion in aged mice compared to controls (Fig. 5A). These findings are in agreement with the results observed in Ca^{2+} signaling and voltage-gated Ca^{2+} currents. A trend towards an increase in basal insulin secretion (0.5 mM G) as well as insulin content (Fig. 5B) was observed in islets from both groups of aged mice, although it was not statistically significant. Analysis of *Ins1* and *Ins2* gene expression by real-time PCR revealed no changes at this level (Fig. 5C).

Ultrastructural features in β-cells from aged and control mice.

To examine potential alterations related with the secretory pathway, we also analyzed electron micrographs from control, aged-HIS and aged-LIS β-cells within pancreatic islets (Fig. 5A). While both the total number of secretory granules per cell (Fig. 5B) and the secretory vesicle density (Fig. 5C) were similar in all groups, the insulin granule diameter was slightly smaller in aged β-cells (Fig. 5E). Moreover, aged-HIS β-cells displayed a modest decrease in the percentage of the characteristic mature dense granules , along with a slightly higher proportion of immature grey secretory vesicles (Fig. 5D). In addition to explore the population of secretory granules, we also noticed increased endoplasmic reticulum (ER) area in aged β-cells of both groups (Fig. 5F). Since increased ER size has been associated with an early adaptive response to ER stress , we analyzed the expression of several markers of the unfolded protein response (UPR) and ER stress. These markers included the ER chaperone BIP (encoded by *Hspa5*), the activating transcription factor 4 (encoded by *Atf4*) and the C/EBP homologous protein (CHOP, encoded by *Ddit3*) (Fig. 5G). We found that, while BIP expression was significantly higher in aged-LIS islets, CHOP and ATF4 expression did not differ among groups. Unlike the ER, we did not find changes either in mitochondrial area or density among groups (Supplementary Fig. 4). These findings suggest that aged β-cells exhibited a mild ER stress.

β-cell mass is enhanced in aged mice.

In agreement with previous studies , the morphological analysis of the pancreas revealed increased β-cell mass as well as expanded islet size with aging (Supplementary Fig. 5). Although these effects were more evident in the aged-LIS group, aged-HIS mice showed a non-significant trend. Augmented β-cell mass was associated with increased pancreas weight in aged mice compared to controls, while β-cell area was not significantly different between

groups (Supplementary Fig. 5). Proliferation in mouse β-cells is characterized by a marked decline with age , while β-cell apoptosis is more feasible to occur during aging . We found ~0.8% and ~0.2% of insulin^{+}/Ki67^{+} β-cells in control and aged mice, respectively (Supplementary Fig. 6), which is consistent with prior findings . Aged-LIS animals also displayed higher proportion of apoptotic β-cells.

DISCUSSION

Studies on the effect of aging on the pancreatic β-cell have generated heterogeneous results in mice, ranging from improved β-cell function to a decline in GSIS or even no changes . This heterogeneity might be due in part to differences in the ages considered, which may lead to confusing interpretations . In several reports, the effects of aging on β-cells were examined in middle-aged animals, when senescence characters are not yet present , or aged mice were compared with juvenile non-mature controls . Another confounding factor is that, because aging is frequently associated with a decline in peripheral insulin sensitivity , the IR-associated compensatory effects on glucose homeostasis and islet secretion may veil those alterations caused by aging. Due to the importance of these key aspects to understand the impact of aging on β-cell function, in the present study we analyzed 3-month-old (controls) and 20-month-old (aged) mice. The latter were classified into two groups according to their degree of insulin sensitivity, which was assessed by the surrogate markers QUICKI and HOMA-IR. Although the hyperinsulinemic-euglycemic clamp is the gold standard for determining peripheral insulin sensitivity , QUICKI and HOMA-IR provide a reasonable estimate of this parameter. A proper correlation between these surrogates and clamp-based measurements has been observed in rodents . Indeed, QUICKI and HOMA-IR have been employed in mouse and aging studies and to classify groups with different insulin sensitivity

. Both indexes allowed us to categorize the aged mice into two groups with different metabolic patterns: aged-LIS mice presented glucose intolerance, lower insulin sensitivity, hyperinsulinemia and impaired *in vivo* GSIS, whereas glucose homeostasis in aged-HIS mice was comparable to that of controls. Thus, our findings suggest that the deteriorated glucose homeostasis frequently reported in aged mice may be more associated with the reduced insulin sensitivity described in these animals rather than the process of aging itself.

Ex vivo experiments showed that aging produces alterations at different steps of the β-cell stimulus-secretion coupling. Consistent with previous reports , glucose-induced NAD(P)H responses were lower in islets from both aged groups, indicating impaired glucose metabolism. Actually, age-related disturbances in the mitochondrial function of human islets have been associated with decreased copy number of mitochondrial DNA, which affects the respiratory chain activity, and with reduced intracellular ATP levels . Thus, our results confirm that aging perturbs β-cell glucose metabolism. Given that K_{ATP} channels are regulated by intracellular ATP levels, it is very likely that the reduced effect of glucose to close these channels in aged β-cells described here was due to their impaired glucose metabolism. This diminished effect of glucose on K_{ATP} channels was greater in the aged-LIS group, indicating that IR could be exacerbating this alteration. Despite this altered K_{ATP} channel activity in aged β-cells, glucose (11 mM) produced a sufficient plasma membrane depolarization to generate action potentials, as revealed by the action currents. Remarkably, aged β-cells exhibited enhanced voltage-gated Ca^{2+} currents, particularly in the aged-LIS group, and augmented glucose-induced Ca^{2+} signals. This is probably a compensatory adaption to the defects in glucose metabolism and K_{ATP} channel activity, thus ensuring insulin secretion. These findings are in line with studies describing increased Ca^{2+} oscillations in aged mouse islets . Additionally, our results showed that these adaptations resulted in enhanced GSIS in both groups of aged islets, in agreement with other studies . Our

experiments of Ca^{2+} synchrony did not support the existence of significant age-associated alterations in cell-to-cell communication. This is in contrast with studies in human islets showing a decline in Ca^{2+} signal coordination (45). Human β-cells form subgroups within the islets with homotypic contacts and, accordingly, Ca^{2+} signals are organized in subregions (45). However, the whole β-cell population behaves as an anatomical and functional syncytium in mouse islets. This particular feature is likely to lead to a more robust cell-to-cell signaling in mice, protecting them against age-associated alterations in intercellular coordination.

Pancreatic β-cells were also examined by electron microscopy. Although we observed minor changes in the diameter and types of secretory granules in the aged β-cells, they were not comparable to those substantial alterations reported in β-cells from IR models . Indeed, these minor changes did not adversely affect insulin secretion or content in aged β-cells at all. Thus, increased GSIS in aged β-cells may be more likely derived from functional adaptive changes at the Ca^{2+} signaling level rather than alterations in the biogenesis of secretory granules. Remarkably, both groups of aged β-cells displayed expanded ER size, which might be related with a higher demand of insulin biosynthesis for secretion . Since augmented ER size has been described as an early step of a sequence of adaptive mechanisms against ER stress, the unfolded protein response (UPR) , we analyzed several ER stress markers. While BiP mRNA levels augmented in the aged-LIS group, no significant differences were found in the expression of either ATF4 or the proapoptotic transcription factor CHOP. Overall, these results indicate that aged β-cells undergo an adaptive UPR that would alleviate their mild ER stress , in agreement with similar findings in T2D patients and diabetic mice . Although this mild ER stress is unlikely to be related to the increased apoptotic rate observed in the aged β-cells, we cannot rule out this possibility. Indeed, islet cell survival seems to be more compromised in aged mice than in young animals, when exposed to ER stressors .

Enhanced β-cell mass and islet expansion have been reported in aged rodents . Consistent with these findings, we observed increased β-cell mass and islet size in aged-LIS mice. Upregulation of β-cell mass is thought to be a compensatory mechanism to IR . Thus, our findings suggest that the lower peripheral insulin sensitivity in aged-LIS animals presumably triggered these morphological adaptations, which would occur in parallel with β-cell functional changes. In the case of the aged-HIS group, expansion of β-cell mass and islet size followed a non-significant tendency towards increase. This trend might represent some adaptation to the enhanced insulin demand due to increased body weight with aging. Actually, the age-associated dynamics of β-cell mass has been also correlated with changes in body weight . Therefore, our findings indicate that aging does not lead to a decline in β-cell mass, but rather allows for β-cell expansion in the setting of IR.

In summary, in the present study we show that glucose-induced inhibition of K_{ATP} channels is attenuated in aged β-cells. This effect was probably associated with reduced glucose metabolism. To preserve their secretory function, both aged-HIS and aged-LIS β-cells compensate for these alterations by enhancing Ca^{2+} influx and insulin release. Such an improvement in β-cell function was sufficient for adequate regulation of glucose homeostasis in aged-HIS mice. However, it was not enough to cope with the lower insulin sensitivity displayed by the hyperinsulinemic and glucose intolerant aged-LIS animals, as shown in several models of IR . Our findings indicate, thus, that β-cell function does not necessarily decline with aging. Rather, mouse aged β-cells can eventually adapt to age-derived disturbances. Therefore, the impaired glucose homeostasis observed in numerous studies in aged mice might not be due to aging but to insufficient adaptation to IR. In any case, further research would be required to assess whether all the age-associated alterations described in the present study, including minor ultrastructural changes, could be more harmful in conditions of chronic IR or metabolic stress such as obesity, thus favoring progression to

T2D. In this regard, it has been reported that aged mice fed a high-fat/high-sucrose western diet for a short term are able to expand β-cell mass and also, that the insulin content and secretion from their pancreatic islets exhibit resistance to the diet-induced functional decline observed in young controls (49). Thus, these findings indicate that aged mice could develop resilience when challenged with certain metabolic conditions. Finally, given that our study was performed in male mice of the C57BL/6 strain, it would be interesting to perform further studies in females and also, in other genetic backgrounds, to obtain a broader insight about the alterations and/or adaptations of pancreatic β-cells during aging. It would be also appealing to explore whether changes in β-cell function during aging could differentially affect peripheral insulin sensitivity in both groups of aged mice.

In humans, glucose homeostasis seems to deteriorate with aging . Since β-cell mass remains well preserved in older adults , this deterioration is probably associated with insufficient compensatory secretion of β-cells with aging, particularly when facing IR This divergence from mice could be due to the longer lifespan of human β-cells : human insulin-secreting cells are expected to be exposed to metabolic stress conditions for longer periods with aging, making them more vulnerable to detrimental effects compared with mice. In any case, our present findings could be also used as a paradigm for the identification and study of the cellular events that may favor the transition to impaired secretory performance in human aged β-cells. This information may be important to understand the higher prevalence of T2D and IGT with aging in older adults.

Acknowledgements.

We thank M.S. Ramon and M.L. Navarro for their expert technical assistance. This research was supported by grants from the Ministerio de Ciencia, Innovación y Universidades, Agencia Estatal de Investigación, Fondo Europeo de Desarrollo Regional (FEDER) and Generalitat Valenciana (BFU2017-86579-R and PROMETEO/2020/006 to AN and BFU2016-77125-R to IQ) and from the Conselho Nacional de Desenvolvimento Científico e Tecnológico (grant No. 304388/2020-3 to AR) and the Programa Institucional de Internacionalização from the Coordenação de Aperfeiçoamento de pessoal de Nível Superior (CAPES). CIBERDEM is an initiative of the Instituto de Salud Carlos III.

Declarations of interests.

The authors have no interests to declare.

Author contributions.

E.T. and I.Q. contributed to the conception or design of the work; E.T., S.S., L.A. and A.G.H. contributed to the acquisition, analysis and interpretation of data; E.T., S.S., A.R., P.A.M., A.N. and I.Q. contributed to the discussion; E.T. and I.Q. drafted the manuscript. All authors reviewed the manuscript and approved the final version of the article.

REFERENCES

REFERENCES

1. Crimmins EM. Lifespan and healthspan: Past, present, and promise. *Gerontologist*. 2015;55(6):901-911. doi:10.1093/geront/gnv130.

2. Shimokata H, Muller DC, Fleg JL, Sorkin J, Ziemba AW, Andres R. Age as independent determinant of glucose tolerance. *Diabetes*. 1991;40(1):44-51. doi:10.2337/diab.40.1.44.

3. Chia CW, Egan JM, Ferrucci L. Age-related changes in glucose metabolism, hyperglycemia, and cardiovascular risk. *Circ Res*. 2018;123(7):886-904. doi:10.1161/CIRCRESAHA.118.312806.

4. IDF 2019. International Diabetes Federation. IDF Diabetes Atlas, 9th edition. http://www.diabetesatlas.org.

5. Alejandro EU, Gregg B, Blandino-Rosano M, Cras-Méneur C, Bernal-Mizrachi E. Natural history of β-cell adaptation and failure in type 2 diabetes. *Mol Aspects Med*. 2015;42:19-41. doi:10.1016/j.mam.2014.12.002.

6. Petersen KF, Morino K, Alves TC, et al. Effect of aging on muscle mitochondrial substrate utilization in humans. *Proc Natl Acad Sci U S A*. 2015;112(36):11330-11334. doi:10.1073/pnas.1514844112.

7. Ehrhardt N, Cui J, Dagdeviren S, et al. Adiposity-Independent Effects of Aging on Insulin Sensitivity and Clearance in Mice and Humans. *Obesity (Silver Spring)*. 2019;27(3):434-443. doi:10.1002/oby.22418.

8. González-Rodríguez Á, Más-Gutierrez JA, Mirasierra M, et al. Essential role of

protein tyrosine phosphatase 1B in obesity-induced inflammation and peripheral insulin resistance during aging. *Aging Cell*. 2012;11(2):284-296. doi:10.1111/j.1474-9726.2011.00786.x.

9. Li L, Trifunovic A, Kohler M, et al. Defects in β-Cell Ca2+ Dynamics in Age-Induced Diabetes. *Diabetes*. 2014;63(12):4100-4114. doi:10.2337/db13-1855.

10. Aguayo-Mazzucato C, van Haaren M, Mruk M, et al. beta Cell Aging Markers Have Heterogeneous Distribution and Are Induced by Insulin Resistance. *Cell Metab*. 2017;25:898-910 e5. doi:10.1016/j.cmet.2017.03.015.

11. Xiong Y, Yepuri G, Necetin S, Montani JP, Ming XF, Yang Z. Arginase-II promotes tumor necrosis factor-α release from pancreatic acinar cells causing β-cell apoptosis in aging. *Diabetes*. 2017;66(6):1636-1649. doi:10.2337/db16-1190.

12. Mohamad M, Mitchell SJ, Wu LE, et al. Ultrastructure of the liver microcirculation influences hepatic and systemic insulin activity and provides a mechanism for age-related insulin resistance. *Aging Cell*. 2016;15(4):706-715. doi:10.1111/acel.12481.

13. Chow HM, Shi M, Cheng A, et al. Age-related hyperinsulinemia leads to insulin resistance in neurons and cell-cycle-induced senescence. *Nat Neurosci*. 2019;22(11):1806-1819. doi:10.1038/s41593-019-0505-1.

14. Montanya E, Nacher V, Biarnes M, Soler J. Linear correlation between β-cell mass and body weight throughout the lifespan in Lewis rats. Role of β-cell hyperplasia and hypertrophy. *Diabetes*. 2000;49(8):1341-1346. doi:10.2337/diabetes.49.8.1341.

15. Xin Y, Okamoto H, Kim J, et al. Single-Cell RNAseq reveals that pancreatic β-cells from very old male mice have a young gene signature. *Endocrinology*. 2016;157(9):3431-3438. doi:10.1210/en.2016-1235.

16. Kehm R, König J, Nowotny K, et al. Age-related oxidative changes in pancreatic islets are predominantly located in the vascular system. *Redox Biol*. 2018;15(December 2017):387-393. doi:10.1016/j.redox.2017.12.015.

17. Santulli G, Lombardi A, Sorriento D, et al. Age-related impairment in insulin release: The essential role of β 2-adrenergic receptor. *Diabetes*. 2012;61(3):692-701. doi:10.2337/db11-1027.

18. Almaça J, Molina J, Arrojo e Drigo R, et al. Young capillary vessels rejuvenate aged pancreatic islets. *Proc Natl Acad Sci*. 2014;111(49):17612-17617. doi:10.1073/pnas.1414053111.

19. Avrahami D, Li C, Zhang J, et al. Aging-Dependent Demethylation of Regulatory Elements Correlates with Chromatin State and Improved β Cell Function. *Cell Metab*. 2015;22(4):619-632. doi:10.1016/j.cmet.2015.07.025.

20. Gregg T, Poudel C, Schmidt BA, et al. Pancreatic β-cells from mice offset age-associated mitochondrial deficiency with reduced KATP channel activity. *Diabetes*. 2016;65(9):2700-2710. doi:10.2337/db16-0432.

21. Flurkey K, Currer JM, Harrison DE. The Mouse in Aging Research. In: Fox JG, et al, ed. *The Mouse in Biomedical Research (2nd Edition).* American College Laboratory Animal Medicine (Elsevier), Burlington, MA, 2007:637-672.

22. Mather K. Surrogate measures of insulin resistance: of rats , mice , and men. *Am J Physiol Endocrinol Metab*. 2009;296(2):E398-9. doi:10.1152/ajpendo.90889.2008.

23. Lee S, Muniyappa R, Yan X, et al. Comparison between surrogate indexes of insulin sensitivity and resistance and hyperinsulinemic euglycemic clamp estimates in mice. *Am J Physiol Endocrinol Metab*. 2007;294(2):E261-E270.

doi:10.1152/ajpendo.00676.2007.

24. Hauth JC, Clifton RG, Roberts JM, et al. Maternal insulin resistance and preeclampsia. *Am J Obstet Gynecol*. 2011;204(4):327.e1-327.e6. doi:10.1016/j.ajog.2011.02.024.

25. Tudurí E, Bruin JE, Denroche HC, Fox JK, Johnson JD, Kieffer TJ. Impaired Ca2+ Signaling in β-Cells Lacking Leptin Receptors by Cre-loxP Recombination. *PLoS One*. 2013;8(8). doi:10.1371/journal.pone.0071075.

26. Gonzalez A, Merino B, Marroquí L, et al. Insulin hypersecretion in islets from diet-induced hyperinsulinemic obese female mice is associated with several functional adaptations in individual β-cells. *Endocrinology*. 2013;154(10):3515-3524. doi:10.1210/en.2013-1424.

27. Bradford M. A Rapid and Sensitive Method for the Quantitation of Microgram Quantities of Protein Utilizing the Principle of Protein-Dye Binding. *Anal Biochem*. 1976;72(1-2):248-254. doi:10.1006/abio.1976.9999.

28. Marroqui L, Martinez-Pinna J, Castellano-Muñoz M, et al. Bisphenol-S and Bisphenol-F alter mouse pancreatic β-cell ion channel expression and activity and insulin release through an estrogen receptor ERβ mediated pathway. *Chemosphere*. 2021;265. doi:10.1016/j.chemosphere.2020.129051.

29. Martinez-Pinna J, Marroqui L, Hmadcha A, et al. Oestrogen receptor β mediates the actions of bisphenol-A on ion channel expression in mouse pancreatic beta cells. *Diabetologia*. 2019;62(9):1667-1680. doi:10.1007/s00125-019-4925-y.

30. Montanya E, Téllez N. Pancreatic remodeling: Beta-cell apoptosis, proliferation and neogenesis, and the measurement of beta-cell mass and of individual beta-cell size. *Methods Mol Biol*. 2009;560:137-158. doi:10.1007/978-1-59745-448-3_11.

31. Spurr AR. A low-viscosity epoxy resin embedding medium for electron microscopy. *J Ultrasructure Res*. 1969;26(1-2):31-43. doi:10.1016/S0022-5320(69)90033-1.

32. Pfaffl MW. A new mathematical model for relative quantification in real-time RT-PCR. *Nucleic Acids Res.* 2001;29(9):e45. doi:10.1093/nar/29.9.e45.

33. Andrikopoulos S, Blair AR, Deluca N, Fam BC, Proietto J. Evaluating the glucose tolerance test in mice. *Mar Drugs*. 2008;14(12):1323-1332. doi:10.1152/ajpendo.90617.2008.

34. Rorsman P, Ashcroft FM. Pancreatic β-Cell Electrical Activity and Insulin Secretion: Of Mice and Men. *Physiol Rev*. 2018;98(1):117-214. doi:10.1152/physrev.00008.2017.

35. Villamayor L, Rodríguez-Seguel E, Araujo R, et al. GATA6 controls insulin biosynthesis and secretion in adult β-cells. *Diabetes*. 2018;67(3):448-460. doi:10.2337/db17-0364.

36. Marchetti P, Bugliani M, Lupi R, et al. The endoplasmic reticulum in pancreatic beta cells of type 2 diabetes patients. *Diabetologia*. 2007;50(12):2486-2494. doi:10.1007/s00125-007-0816-8.

37. Stolovich-Rain M, Hija A, Grimsby J, Glaser B, Dor Y. Pancreatic beta cells in very old mice retain capacity for compensatory proliferation. *J Biol Chem*. 2012;287(33):27407-27414. doi:10.1074/jbc.M112.350736.

38. Mihailidou C, Chatzistamou I, Papavassiliou AG, Kiaris H. Modulation of Pancreatic Islets' Function and Survival During Aging Involves the Differential Regulation of Endoplasmic Reticulum Stress by p21 and CHOP. *Antioxidants Redox Signal*. 2017;27(4):185-200. doi:10.1089/ars.2016.6671.

39. Helman A, Klochendler A, Azazmeh N, et al. p16Ink4a-induced senescence of pancreatic beta cells enhances insulin secretion. *Nat Med*. 2016;22(4):412-420. doi:10.1038/nm.4054.

40. Kim JK. Hyperinsulinemic-euglycemic clamp to assess insulin sensitivity in vivo. *Methods Mol Biol*. 2009;560:221-238. doi:10.1007/978-1-59745-448-3_15.

41. Corrales P, Vivas Y, Izquierdo-Lahuerta A, et al. Long-term caloric restriction ameliorates deleterious effects of aging on white and brown adipose tissue plasticity. *Aging Cell*. 2019;18(3). doi:10.1111/acel.12948.

42. Badenes M, Amin A, González-García I, et al. Deletion of iRhom2 protects against diet-induced obesity by increasing thermogenesis. *Mol Metab*. 2020;31:67-84. doi:10.1016/j.molmet.2019.10.006.

43. Ihm SH, Matsumoto I, Sawada T, et al. Effect of donor age on function of isolated human islets. *Diabetes*. 2006;55(5):1361-1368. doi:10.2337/db05-1333.

44. Cree LM, Patel SK, Pyle A, et al. Age-related decline in mitochondrial DNA copy number in isolated human pancreatic islets. *Diabetologia*. 2008;51(8):1440-1443. doi:10.1007/s00125-008-1054-4.

45. Westacott MJ, Farnsworth NL, St Clair JR, et al. Age-Dependent Decline in the Coordinated [Ca2+] and Insulin Secretory Dynamics in Human Pancreatic Islets. Diabetes. 2017;66(9):2436-2445. doi: 10.2337/db17-0137.

46. Alarcon C, Boland BB, Uchizono Y, et al. Pancreatic β-cell adaptive plasticity in obesity increases insulin production but adversely affects secretory function. *Diabetes*. 2016;65(2):438-450. doi:10.2337/db15-0792.

47. Herbert TP, Laybutt DR. A reevaluation of the role of the unfolded protein response in islet dysfunction: Maladaptation or a failure to adapt? *Diabetes*. 2016;65(6):1472-1480. doi:10.2337/db15-1633.

48. Collins SC, Hoppa MB, Walker JN, et al. Progression of diet-induced diabetes in C57BL6J mice involves functional dissociation of Ca2(+) channels from secretory vesicles. *Diabetes*. 2010;59(5):1192-1201. doi:10.2337/db09-0791.

49. De Leon ER, Brinkman JA, Fenske RJ, et al. Age-Dependent Protection of Insulin Secretion in Diet Induced Obese Mice. *Sci Rep*. 2018;8(1):17814. doi: 10.1038/s41598-018-36289-0.

50. Saisho Y, Butler AE, Manesso E, Elashoff D, Rizza RA, Butler PC. β-Cell mass and turnover in humans: Effects of obesity and aging. *Diabetes Care*. 2013;36(1):111-117. doi:10.2337/dc12-0421.

51. Chang AM, Halter JB. Aging and insulin secretion. *Am J Physiol Endocrinol Metab*. 2003;284(1):E7-12. doi:10.1152/ajpendo.00366.2002.

52. Cnop M, Hughes SJ, Igoillo-Esteve M, et al. The long lifespan and low turnover of human islet beta cells estimated by mathematical modeling of lipofuscin accumulation. *Diabetologia*. 2010;53(2):321-330. doi:10.1007/s00125-009-1562-x.

FIGURE LEGENDS

Figure 1. Aged-LIS mice display hyperinsulinemia, impaired GSIS and glucose intolerance. *In vivo* measurements of **A)** QUICKI and **B)** HOMA-IR in control (n=35), aged-HIS (n=15) and aged-LIS (n=26) mice. **(C)** Insulin tolerance test after 6 h fasting (n= 13, 6 and 7 for control, aged-HIS and aged-LIS mice, respectively). Area under the curve (AUC) is represented at the right. Fasting (6 h) blood glucose **(D)** and plasma insulin levels **(E)** in control (n=35), aged-HIS (n=15) and aged-LIS (n=26) mice. **F)** Intraperitoneal glucose tolerance test was performed in response to a glucose load of 2 g/kg body weight after a 6-h fast (control, n=33; aged-HIS, n=11; aged-LIS, n=21). AUC is represented at the right. Plasma insulin levels **(G)** and C-peptide levels **(H)** were measured at different time points after an intraperitoneal glucose injection of 2 g/kg body weight in 6 h fasted mice (for insulin measurements: control, n=6; aged-HIS, n=5; aged-LIS, n=6; for C-peptide measurements: control, n=7; aged-HIS, n=5; aged-LIS, n=7). Data are expressed as mean ± SEM and were analyzed using one-way ANOVA (A and AUC in C), Kruskal-Wallis (B, D, E and AUC in F), and two-way ANOVA (C, F, G, and H). * $p<0.05$, ** $p<0.01$ and *** $p<0.001$, when comparing aged-LIS and/or aged-HIS vs control; ## $p<0.01$ and ### $p<0.001$ when comparing aged-LIS vs aged-HIS.

Figure 2. Reduced glucose-induced inhibition of K_{ATP} channel activity in aged-LIS β-cells. A) Representative single-channel recordings of K_{ATP} channel activity in the presence of 0.5 mM glucose (G), 11 mM G and 100 µM diazoxide. K_{ATP} channel activity was reduced with 11 mM G, while reactivated with diazoxide. Expanded traces at 6 min after application of high glucose (11mM) show the presence of action currents, indicating that glucose induced the depolarization of the membrane potential and the generation of action potentials. **B)** Percentage of K_{ATP} channel activity at 11 mM G respect to 0.5 mM G in control (n=15 β-cells

from 5 mice), aged-HIS (n=12 β-cells from 4 mice) and aged-LIS (n=8 β-cells from 3 mice). **C)** Average intracellular NAD(P)H recordings from control, aged-HIS and aged-LIS islets in response to 0.5 mM glucose (G) and 11 mM G. Sodium azide (NaN_3) was applied to obtain a maximal level of $NAD(P)^+$ reduction. **D)** Graph plotting the percentage of AUC per minute in response to 11 mM G and normalized to the maximal reduction level obtained with NaN_3 (control, n=20 islets from 3 mice; aged-HIS, n=18 islets from 3 mice; aged-LIS, n=17 islets from 3 mice). Data are expressed as mean ± SEM and analyzed by one way-ANOVA. **p<0.01 and **** p<0.0001 as indicated; # p<0.05 when comparing with control at 11 mM G.

Figure 3. Voltage-gated Ca^{2+} currents and glucose-induced Ca^{2+} signals are enhanced in aged β-cells. A) Representative recordings of voltage-gated K^+ and voltage-gated Ca^{2+} currents in response to 500 ms depolarizing pulses (-60 mV to +80 mV from a holding potential of -70mV (inset)) in control, aged-HIS and aged-LIS β-cells. The expanded traces in aged-HIS β-cells show the outward K^+ and inward Ca^{2+} currents induced by depolarization. **B)** Average relationship between peak voltage-gated K^+ current density (currents in pA normalized to cell size in pF) and voltage of pulses in control (n=17 β-cells from 5 mice), aged-HIS (n=27 β-cells from 4 mice) and aged-LIS (n=18 β-cells from 3 mice) animals. **C)** Average relationship between voltage-gated Ca^{2+} current density (currents in pA normalized to cell size in pF) and voltage of pulses in control (n=10 β-cells from 5 mice), aged-HIS (n=25 β-cells from 4 mice) and aged-LIS (n=14 β-cells from 3 mice). Data are expressed as mean ± SEM and analyzed by two-way repeated-measures ANOVA (B and C). *p<0.05 and **p<0.01. **D)** Representative traces of intracellular Ca^{2+} in a control islet in the presence of 0.5 mM glucose (G; basal non-stimulatory glucose concentration), 11 mM G (stimulatory glucose concentration), and 30 mM KCl (depolarizing concentration). **E)** Basal fluorescence

at 0.5 mM G. **F, G)** Fluorescence increase ($\Delta F_{340/380}$) (F) and area under the curve (AUC) (G) in response to glucose. **H)** Fluorescence increase ($\Delta F_{340/380}$) in response to KCl. Control: n=22 islets from 3 mice; aged-HIS: n=20 islets from 3 mice; aged-LIS: n=18 islets from 3 mice. Data are expressed as mean ± SEM and analyzed by one-way ANOVA (F-H) and Kruskal-Wallis (E). **p<0.01 and ***p<0.001.

Figure 4. Aged pancreatic islets display enhanced glucose-stimulated insulin secretion. **A)** *Ex vivo* GSIS was performed in batches of freshly isolated size-matched islets exposed to both low (0.5 mM) and high (11 mM) glucose (G). Insulin secretion was normalized by total islet protein levels (control: n=11 from 5 mice; aged-HIS: n=7 from 3 mice; aged-LIS: n=14 from 5 mice). **B)** Islet insulin content normalized by total islet protein levels (control: n=11 from 5 mice; aged-HIS: n=6 from 3 mice; aged-LIS: n=13 from 5 mice). **C)** Islet mRNA levels of *Ins1* and *Ins2* normalized by the housekeeping gene *Hprt* (n=5 mice/group). Data are expressed as mean ± SEM and analyzed by two-way ANOVA (A), one-way ANOVA (B and C) and paired Student's t-test (in (A), to compare each independent group of mice at low and high glucose). *p<0.05, ***p<0.001, #p<0.05, ##p<0.01 and ###p<0.001.

Figure 5. Ultrastructure of control and aged β-cells in electron micrographs. A) Representative electron micrographs of control, aged-HIS and aged-LIS β-cells. Scale bar= 2 µm (upper panel) and 1 µm (medium and lower panel). **B)** Insulin granules per cell. **C)** Granule density. **D)** Percentage of dense, grey, empty and rod-like granules. **E)** Insulin granule diameter. **F)** Percentage of endoplasmic reticulum area. Control: n=19 β-cells; aged-HIS: n=14 β-cells; aged-LIS: n=12 β-cells, from 3 mice per group. **G)** Islet mRNA levels of BIP (*Hspa5*), CHOP (*Ddit 3*) and ATF4 normalized by the housekeeping gene *Hprt* (n=5 per group). Data are expressed as mean ± SEM and analyzed by one-way ANOVA (B, F, G), Kruskal-Wallis (C, E) and two-way ANOVA (D), *p<0.05, **p>0.01, ***p<0.001. M: mitochondria; N: nucleus; ER: endoplasmic reticulum; SG: secretory granules. Black arrows: immature granules; dashed line: plasma membrane.

Figure 1

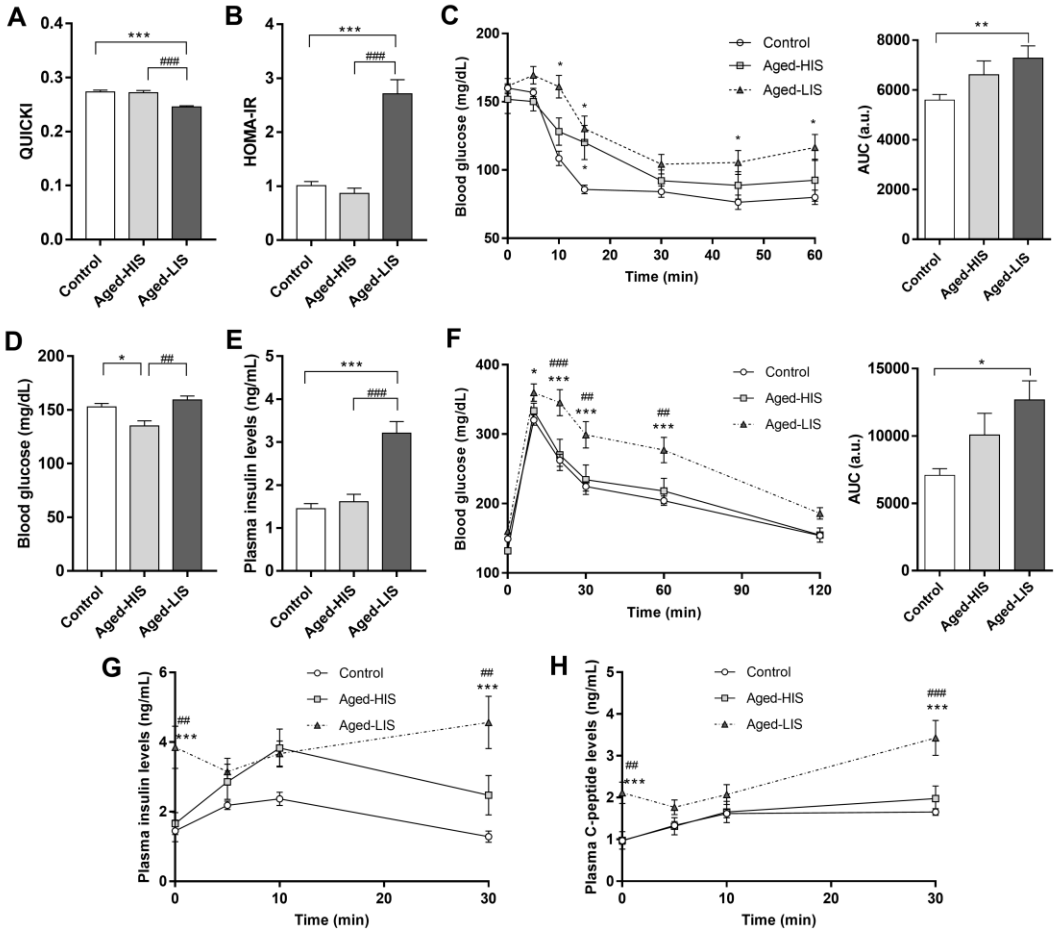

Figure 2

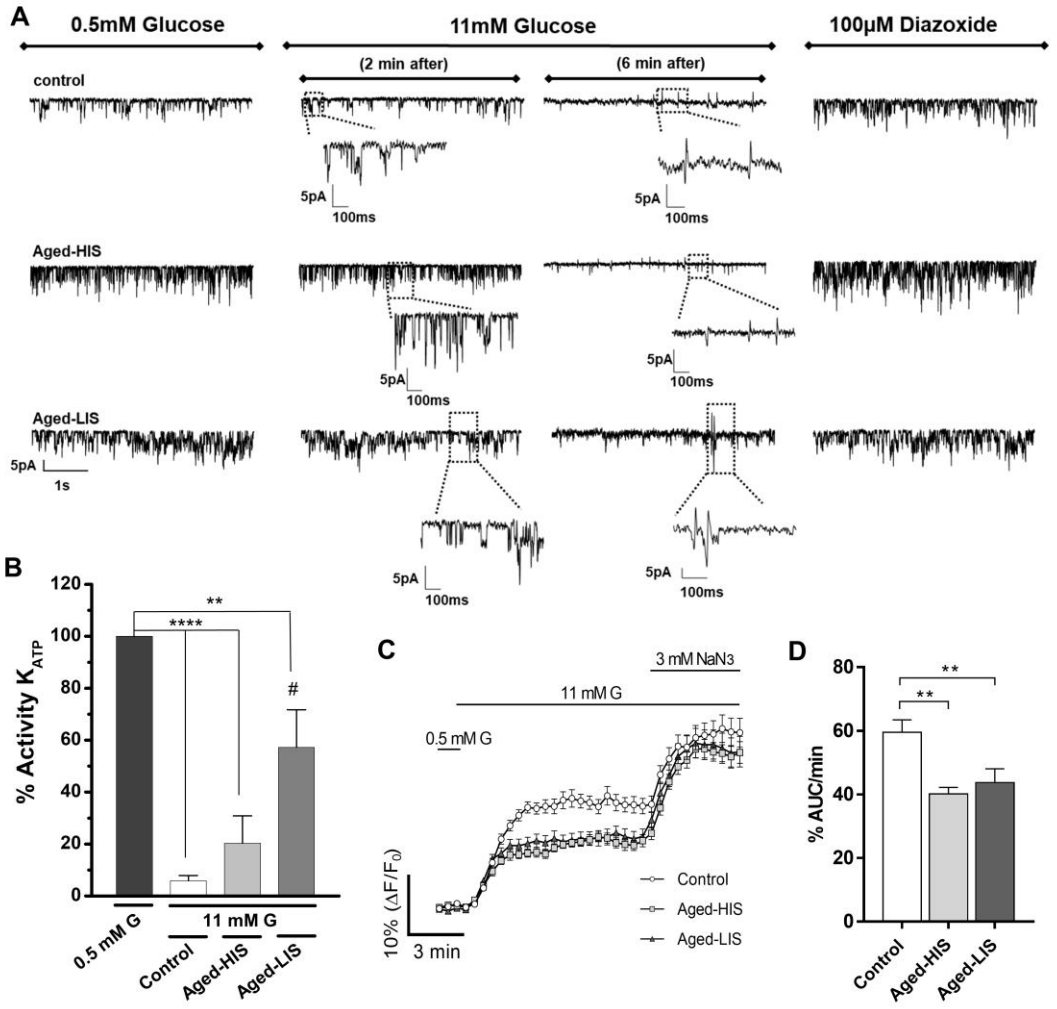

Figure 3

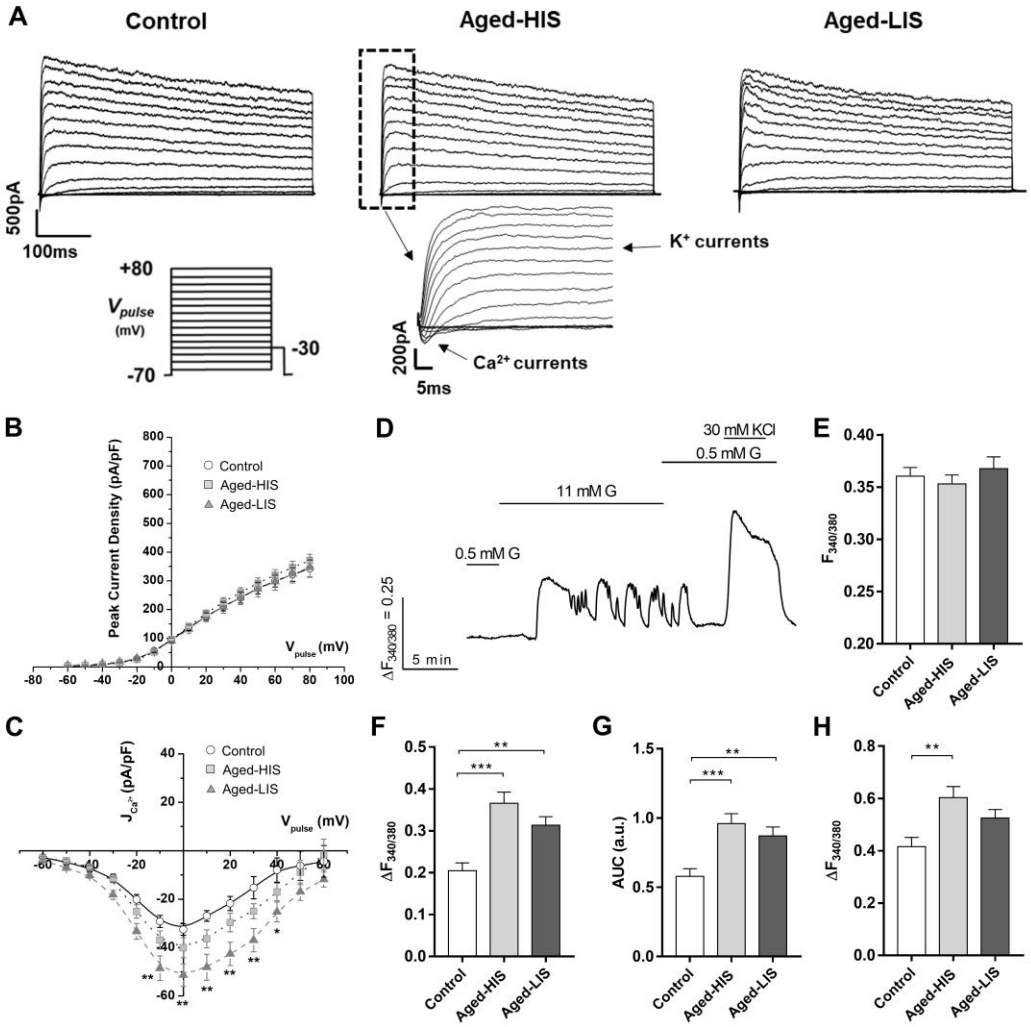

Figure 4

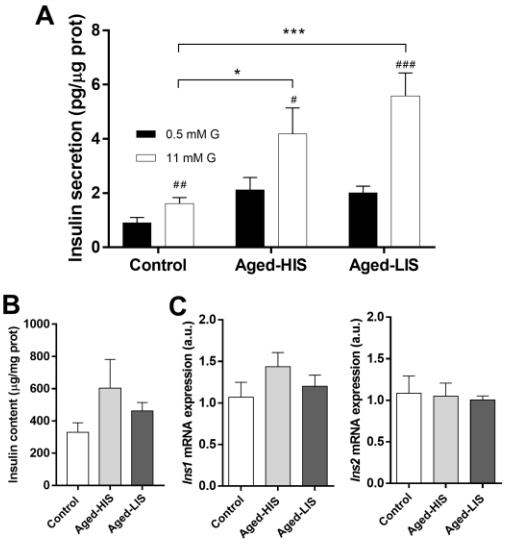

Figure 5